STUDIES AND OPTIMIZATIONS OF DIFFUSION AND EFFUSION IN TRIUMF'S ISAC TARGETS

BY

ROHAN NUTTALL

B.Sc. Honours Physics, University of British Columbia

Thank you to my supervisors Aurelia Laxdal, James Charbonneau and Peter Kunz for guiding me throughout the process of this project. Their support and feedback on the development of this work was invaluable. I would like to thank Mario Santana Leitner for his patience and helpfulness as I navigated RIBO. Furthermore, thank you to Luca Egoriti for his ideas and openness to discussion. I would also like to acknowledge Vesna Sossi, TRIUMF and the UBC Department of Physics and Astronomy for the opportunity to pursue this project.

Abstract

Comprising three main parts, the aim of this thesis is to provide a detailed description and analysis of the physical processes associated with isotope release at TRIUMFs ISAC facility. First, end-to-end simulations of the current target design that integrate all processes (diffusion, effusion, ionization and ionic transport in vacuum, as well as temperature, desorption/adsorption, surface shape and opacity constraints) have been conducted and the results are discussed. Second, drawing from studies conducted at CERN, IFNL-LNL and SCK-CEN, a comprehensive description of the physics and design considerations is provided and a literature review of the best practices for optimizing the (often antagonistic) release parameters is carried out. Third, the current target system was optimized for specific use cases and a discussion of the simulation results is provided. The project consists of the use of analytical models and Monte Carlo simulations to analyze and optimize the production of radioactive ion beams. The RIBO software (developed by Mario Santana Leitner, CERN) is used to optimize the interior target geometry (made of tantalum foils) specifically for the release of Li^{8}, Li^{9} and Li^{11} isotopes.

Table of Contents

List of Tables

List of Figures

1 Introduction

Radioactive isotopes (also referred to as radioisotopes, radionuclides, exotic species or short-lived isotopes) are forms of elements that vary in neutron number. The range of applications of the unique properties of radioactive isotopes is considerable; spanning materials science, cutting edge astrophysical nuclear interaction and reaction modeling, fundamental symmetry studies, research in nuclear isomers research, and applied therapeutic and diagnostic usages in the medical sciences. However, these chemical species do not occur naturally on Earth and must be produced at a particle accelerator or nuclear reactor.

The Isotope Separator and Accelerator (ISAC) at TRIUMF is an isotope separation on-line (ISOL) facility that uses a primary proton beam (500 MeV and up to 100μA) to drive nuclear reactions within targets heated to high temperatures. These nuclear reactions spawn a variety of radioactive isotopes within the target material and the short-lived nuclides then migrate to a transfer line where they are ionized and accelerated by a series of electrostatic electrodes. This secondary radioactive ion beam (RIB) is then directed to a mass separator where a specific isotope can be selected and guided with a transport system to various experiments.

Extremely low production cross-sections, overwhelming production of unwanted species and very short half-lives of the nuclei of interest are the primary inhibiting factors behind the provision of intense exotic beams. Therefore, it is of considerable interest to develop an understanding of the means by which efficiency improvements can be made to ensure large enough quantities arrive at the final location where they are being studied or applied.

1.1 Key concepts and parameters of interest

The ultimate aim for ISOL systems is the production of beams of exotic nuclei that are abundant, pure, and of good ion optical quality. The whole production sequence requires:

1. High production rate: the production cross-section, or probability that a reaction will take place, is energy dependent and so targets must be

designed to handle the power deposition associated with high beam intensities.

2. Speed and Efficiency: production rate of exotic nuclei will always be marginal [21]. Hence, the manipulation of reaction products; release, ionization, selection and transport has to be very efficient to ensure that losses due to decay from the moment of production to the arrival at the experiment is kept to a minimum.

1.1.1 Production

The function of the target is to produce RIBs. Due to the stochastic nature of the nuclear processes inside of the target material, accurately predicting the yield of the desired isotope is requires a tool that can handle complex physical and chemical models. As many problems in physics involve describing or simulating the motion of particles through space, higher dimensional problems can be computationally expensive to solve numerically [1] and are best suited for a Monte Carlo (MC) code. Developed at the Los Alamos National Laboratory in 1940 [11], the MC method relies on random sampling to approximate deterministic problems. As yield predictions are essentially particle transport and interaction predictions, they can be estimated by MC simulation.

FLUKA is a multi-purpose particle physics simulation tool that uses Monte Carlo statistics to treat a wide variety of physics cases, ranging from high energy experimental physics and engineering, shielding, detector and telescope design, cosmic ray studies, dosimetry, medical physics, and radio-biology [4], [6]. The software is well-suited to providing reliable results for in-target isotope production rates by simulating the interactions and transport of different particles with and through matter and has a history of extensive use at TRIUMF. The user provides inputs such as incident particle energy and geometry parameters and is able to extract results such as energy deposition and secondary particle production. The beam can be defined according to direction and distribution (typically Gaussian) while the geometry must be implemented using Boolean operations and quadric surfaces to create finite spatial regions with the flair graphical user interface.

It should be noted that there are a variety of computational models and nuclear cascade codes that characterize inelastic particle-nucleus collisions according to different models, each with their respective limits on conditions for validity [5]. The in-target production values obtained using one code may be vastly different from another and this uncertainly must be taken into account when predicting yields from in-target production rates. Luckily, for diffusion and effusion studies, the discrepancy between model values is independent of

the release efficiency. This is because diffusion and effusion takes place after production and so the initial number of species present can be set to an arbitrary constant. Hence, one can optimize targets independent of knowing the 'true' in-target production values. It should be noted that beam deposition and target heating does play a role and is an important parameter to consider for target lifetime (temperature effects will be discussed further in Chapter 2).

1.1.2 Speed and Efficiency

The current target design in the ISAC facility comprises a 3.4 cm long target that sits in the middle of a pure tantalum container. The target itself is constructed out of 470 tantalum foils each having a thickness of 25 μm, dimpled and tightly pressed together. The reason for this structure is to ensure that once the isotopes are produced within the target bulk, they are able to diffuse rapidly to the surface of a given foil and then drift through the voids between the foils towards the extraction tube. The system is held under vacuum (10^{-3} Pa) to allow for the birthed nuclei to travel unimpeded by residual gas particles as they drift through the interior geometry—a process known as effusion. The ISAC system's ionizer is a surface ion source (SIS) which means that nuclei become thermally ionized upon contact with the section of the transfer tube that has a sufficiently high work function (currently a 10 mm by 10 mm rhenium foil that is rolled and inserted into the end of the extraction tube). Coupled to each of these design considerations is an associated efficiency, meaning that target optimization of diffusion, effusion and ionization is a highly geometry dependent problem [31].

The yield of a radioactive isotope beam yield is expressed as the four-factor product for the final intensity [12]:

$$I({}^{A}_{Z}X^{+})_{RIB} = I(p^{+}) \cdot [\epsilon_{p^{+}\rightarrow {}^{A}_{Z}X} \cdot \epsilon_{Diff} \cdot \epsilon_{Eff} \cdot \epsilon_{({}^{A}_{Z}X\rightarrow {}^{A}_{Z}X^{+})}]$$

- $I({}^{A}_{Z}X^{+})_{RIB}$ is the secondary radioactive beam exiting the target.
- $I(p^{+})$ is the primary proton beam impinging on the target.
- $\epsilon_{(p^{+}\rightarrow {}^{A}_{Z}X)}$ is the efficiency of producing species X from the initial proton beam p^{+} (however, it is usually expressed in terms of cross section).
- $\epsilon_{diff} \cdot \epsilon_{eff}$ are the factors associated with extracting the radioactive isotopes after in-target production.
- $\epsilon_{({}^{A}_{Z}X\rightarrow {}^{A}_{Z}X^{+})}$ is the ionization efficiency.

There are other efficiency parameters associated with the delivery of isotopes from production to experiment such as $\epsilon_{transport}$ (transport through the beamline system after exiting the ionizer), $\epsilon_{separation}$ (electromagnetic mass selection), $\epsilon_{storage}$ (storage, cooling and bunching, occasionally required), and $\epsilon_{post-acc}$ (post-acceleration, if required) [37]. While these factors are relevant (especially for isotopes with half-lives on the order of milliseconds) they will be taken to be unity here as this thesis concerns only the target geometry, not the additional systems and subsystems of beam delivery. To complicate matters, even within the parameters we wish to consider, it is important to understand that their efficiencies dont all have the same dependencies and range. For an order of magnitude approximation, $\epsilon_{({}^{A}_{Z}X \rightarrow {}^{A}_{Z}X^{+})}$ can range from 0.1% to 90% while $\epsilon_{diff} \cdot \epsilon_{eff}$ can be as low as 10^{-6}% for some isotopes [37]. The intersecting dependencies of the efficiency parameters in question presents a global optimization problem where the maximization of one may lead to the minimization of other. For instance, while one may be inclined to simply maximize $I(p^{+})$, the increased beam deposition power could overcome the targets ability to dissipate the heat, resulting in sintering or melting which would lower the release properties [27].

Release Fraction:

The $\epsilon_{diff} \cdot \epsilon_{eff}$ is often called the release efficiency, ϵ_R, and is expressed (for the i^{th} particle) as [30]:

$$\epsilon_R^i = e^{\frac{-t_{tot}^i ln(2)}{T_{1/2}}} \tag{1.1}$$

where $T_{1/2}$ is the half-life of the isotope in question. Taking into consideration sticking (or dwell) time, which is the time that a radioactive atom sticks to a surface in the geometry before desorbing back into the void, the individual total release time of particle is $t_{tot}^i = t_{diff} + t_{eff} + N_{collisions} \cdot t_s$, where $N_{collisions}$ is the number of collisions a given particle suffers while effusing through the target and t_s is the sticking time. Such times can either be sampled from a probability distribution or merely taken to be an average. Then, the remaining fraction represents the quantity of isotopes that have survived half-life decay after $t = t_{tot}$. The time elapsed from production to extraction (release) to the ion source is also known as the total delay time.

In order to compute the global release fraction, ϵ_R, we must integrate the intrinsic release function multiplied by the individual release probability [12]. This function is given by the convolution (denoted by the operator, $*$) of the diffusion release function, $DF(t)$, and the effusion release function, $E(t)$, (obtained from a probabilistic analysis of the release times of a given simulation).

The functional form of this integral is:

$$\epsilon_R = \int_0^\infty DF(t) * E(t) \cdot e^{\frac{-t^i_{tot} ln(2)}{T_{1/2}}} dt \tag{1.2}$$

While this equation will be treated in greater depth in the subsequent pages, it is introduced here so as to clear any ambiguities surrounding what is meant by release efficiency or release fraction. It is useful to note that while diffusion and effusion can be decoupled to extract separate efficiency parameters, the ionization efficiency cannot be [30].

In summary, a description of the physical process associated with isotope release from the target is:

- Isotopes are generated within the 25μm tantalum foils from the interaction with a proton beam of current I_{p+}.
- They diffuse through the target matrix until reaching the grain boundary and desorb into the vacuum between successive foils. This takes time t_{diff} on average.
- The neutral isotopes then effuse through the free space between foils, colliding with foils and sticking to them for t_s. This process takes time t_{eff} $+N_{collisions} \cdot t_s$.
- The isotopes become ionized after reaching the ion source and are subsequently transported to the beamline system.

1.1.3 Diffusion

The principal delay process associated with isotope release is diffusion [28]. This is because the timescale of fragments produced within the target bulk migrating to the surface of the material (mainly by interstitial jumps) is typically orders of magnitude larger than effusion. For a given homogeneous distribution of a radioactive isotope inside a target, the time it takes for the isotope to escape to the surface of the foil is governed by Fick's second law [7]:

$$\frac{\partial C(\vec{r},t)}{\partial t} = D(T)\nabla^2 C(\vec{r},t) \tag{1.3}$$

where $\vec{r}$ is a 3D space vector, t is time, C is concentration in units $\left[\frac{numberofatoms}{volume}\right]$, and $D(T)$ is the diffusion coefficient as a function of temperature.

The diffusion constant $D(T)$ depends on the diffusing species, substrate and the temperature. The temperature dependence is given by the Arrhenius equation and the pre-exponential factor is typically found from experimental measurements [17]:

$$D(T) = D_0 e^{\frac{-\Delta H}{k_B T}} \tag{1.4}$$

where D_0 is the maximum diffusion constant, ΔH is the enthalpy of activation for diffusion, k_B is the Boltzmann constant and T is temperature.

By assuming the flow direction to be normal to the surface, Equation 1.3 can be solved analytically for simple geometries such as planar slabs/foils, cylindrical fibers, and spherical particles [23]. However, several assumptions have to be made about the boundary and initial conditions to make the solution tractable:

- The initial concentration profile $C(\vec{r}, 0)$ is constant. That is, the fragments are assumed to be birthed isotropically.
- The diffusion constant is assumed to be homogeneous and constant (no spatial or temporal dependence).
- For thin foils, $\vec{r} \to x$ (one-dimensional diffusion). In this regime, Equation 1.3 becomes 1.6.
- A uniform temperature distribution is assumed.

The solution of the diffusive flux for thin foils, derived by M. Fujioka and Y. Arai [8], is given by:

$$DF(t) = \frac{2n}{\pi^2} \sum_{m=1}^{\infty} \frac{e^{\frac{-(m-1)^2 \cdot t}{\tau_D}}}{(m-1)^2} \tag{1.5}$$

where $\tau_D = \frac{a^2}{\pi^2 D}$ is the diffusion time constant ($2a$ = foil thickness).

The diffusion efficiency is then determined by calculating the total number of isotopes completing the diffusion process without decaying divided by the number of isotopes that were initially produced.

$$\frac{\partial C(x,t)}{\partial t} = D(T) \frac{\partial^2 C(x,t)}{\partial x^2} \tag{1.6}$$

1.1.4 Effusion

Effusion is the thermal transport of atoms under molecular flow. After diffusing to the foil boundary, the radioactive isotopes then desorb from the surface and drift to the exit of the target container. An effusing particle is best described as a particle pursuing a random walk made up of a sequence of straight lines between collisions with the walls and hence it is well treated by a Monte Carlo method. The effusion efficiency, ϵ_{eff}, is given by the total number of isotopes completing the effusion process without decaying divided by the total number of isotopes that completed the diffusion process without decaying. As particles collide with the walls, they are equipped with a certain probability of adsorbing to the surface. They can either desorb after an amount of time (sticking time) or remain condensed to the surface for the remainder of the particle's lifetime.

1.1.5 Ionization

In order to be extracted, shaped into a beam and guided to experiments, effusing radioactive isotopes need to be ionized. After ionization, the particles can be accelerated by electrode and steered by magnets in the beamline system. The ionization efficiency, $\epsilon_{({}^{A}_{Z}X \to {}^{A}_{Z}X^{+})}$, is an important parameter to know as it provides an indication of how well the extraction system works. It is defined by counting, out of all the particles that survive radioactive decay during the diffusion and effusion process, the fraction that end up being extracted from the ion source. This factor is both isotope, substrate and temperature dependent. Indeed, an argument can be made that it is geometry (collision) dependent as well. At TRIUMF, though other mechanisms of promoting ionization are used (such as resonant laser or electron impact ionization), the ion source concerning this study relies on thermal ionization, or surface ionization, to strip electrons from the radioactive nuclei. After ionization, the gas of effusing isotopes forms a plasma. The probability of ionization of a gas particle after each collision at high enough temperature is governed by the Saha-Langmuir equation:

$$\alpha_S = \frac{n_+}{n_0} = \frac{g_+}{g_0} \exp\left(\frac{W - \Delta E_i}{kT}\right) \tag{1.7}$$

where $\frac{n_+}{n_0}$ is the ratio of ions to neutrals, $\frac{g_+}{g_0}$ is the ratio of statistical weights of the first ionic and neutral states, W is the substrate work function, ΔE_i is the ionization potential (both in electron volts), k is Boltzmann's constant and T is temperature in Kelvin. This equation refers to *positive* ionization, however *negative* surface ionization may occur if the ionization potential of the effusing species is much higher than the work function of the substrate. In our case, we are interested in Li^8, Li^9 and Li^{11} isotopes ($\Delta E_i = 5.4$ eV interacting with a rhenium ionizer ($W = 14.5$ eV), so surface ionization will always be positive. It should be noted that the probability of a single surface ionization is given by $\frac{\alpha_S}{\alpha_S+1}$ [12].

For surface ionizers, the likelihood of recombination can be quite high. That is, if an ion collides with the ionizer substrate, it can gain back an electron and become neutral once more. It may then experience further collisions with the probability of being ionized again being given by Equation 1.7. Therefore, in order to have an accurate picture of ion transport, it is necessary to take into consideration the path of effusing atoms and keep track of the number of collisions they suffer along the way. It is known that the surface ionization efficiency can be improved by reducing the dimensions of the ion source, increasing the its aperture while operating it at high temperatures [18], [12].

1.2 Radioactive Isotope Beam Optimizer (RIBO)

In order to accomplish the task of studying and optimizing TRIUMF's ISAC target system, the Radioactive Isotope Beam Optimizer (RIBO) MC code is utilized. Developed in 2005 by Mario Santana Leitner at CERN, the code has since been used and tested by several labs around the world [30], including Oak Ridge National Laboratory in the United States, the Paul Scherrer Institut in Switzerland and Legnaro National Laboratories in Italy. RIBO was built to satisfy the need for a tool that can predict the release of radioactive nuclei from ISOL targets. Over the past 10 years, priority has been given to this task at many labs around the world such as SPES, RIST-ISOLDE and SCK-CEN.

1.2.1 Capabilities

In the distribution sent to TRIUMF, RIBO is capable of integrating the "main phenomena involved isotope extraction and ion beam formation: Diffusion, Effusion, Ionization, Ion Transport" [9]. The code has a diversity of specific collision laws to govern the simulation of effusion, allows interactions with residual atoms to be taken into consideration, and allows the user to define arbitrarily complex 3D geometries. RIBO provides several output options that can provide useful simulation data on how particles behave within target geometries. Furthermore, options for custom FORTRAN routines to match the simulation more precisely to the problem at hand are also included. The principle objective of the code is to forecast different efficiencies, extract physical parameters and spot the factors that hinder release.

Employed in this work are the following functions of RIBO:

- Defining source of radioisotopes.
- Diffusion release curve sampling for currently target material.
- Effusion in intermediate molecular flow through exact target geometry.
- Ionization emulation for more accurate ion transport efficiency calculations.
- Particle tracing, effusion time-share analysis and scatter plots of particle birth location vs. total release time.
- Average emittance maps.
- Extract intrinsic and global release curves.
- Average release time calculations in diffusion and effusion phases.
- 3D visualization of geometry.

After a simulation, RIBO provides the release distribution probability (also called the intrinsic release function). RIBO also provides diffusive-effusion simulation options for carbides, powders and fibers, which may be useful for future work.

1.2.2 Limitations

One of the main features of RIBO that makes it a desirable tool for target studies is the module for computing the estimated release fraction as a function of parameters of interest (such as sticking time, half-life and diffusion time constant). However, the version sent to TRIUMF did not have this capability. The user manual provides a brief description of how to obtain the release fraction values manually, so a routine outside of the program can be easily written to compensate for this.

It should be noted that the last update to the RIBO page on CERN's website (http://ribo.web.cern.ch/) was in 2006. With an inactive userbase, any enquires about the program must be sent to Mario Leitner. There is no robust geometry compiler or graphical user interface and while the "convgeom.sh", "translate.sh" and "rotate.sh" bash-shell scripts aim to provide assistance for building the often large input files, their functions are limited. An online version of RIBO is claimed to exist (http://www.targisol.csic.es/intro ires.html/) however this website has not been maintained and remains inaccessible to potential users.

2 Simulation

A RIBO simulation was built to depict the TRIUMF ISAC target system as accurately as possible. In order to do this, it was required to define the 3D geometry of the target interior, materials, effusing species, ionization conditions, non-uniform temperature profiles, the correct source of particles and electromagnetic fields for ion transport considerations. The physical mechanisms had to be decided and data analysis tools had to be written (in MATLAB, [10]) in order to extract meaningful insights from the simulation data.

2.1 Geometry

2.1.1 Combinatorial Geometry

In RIBO, the target must be described by using combinatorial geometry. This is a branch of geometry that applies combinatorics to study constructive methods of abstract, discrete geometric objects. In our context, these objects may be any geometric shape in $\mathbb{R}^3$ such as a plane, cylinder or sphere. New, more complex objects can then be arranged by defining the manner in which a series of basic shapes intersect with one another. The walls and volumes that the particles produced in the target will interact with can then be created with an astonishingly small basis of shapes.

Cones, cylinders and spheres belong to a family of more general conic surfaces called quadrics expressed by equation 2.1 and plotted in figure 2.1. These polynomials of degree 2 are defined by 9 parameters. Higher order polynomials (quartics and quintics, for example) permit the representation of more complex surfaces, but require vastly more parameters, and hence computing power in the context of a simulation.

$$a \cdot z^2 + b \cdot y^2 + c \cdot z^2 + d \cdot x \cdot y + e \cdot x \cdot z + f \cdot y \cdot z + g \cdot x + h \cdot y + i \cdot z = C \quad (2.1)$$

2.1.2 Defining a simple model

The coefficients given by equation 2.1 are given as geometric entries in the *Surfaces* card for RIBO's input file. To achieve a suitable comparison and minimize debugging, the full target geometry is implemented in stages.

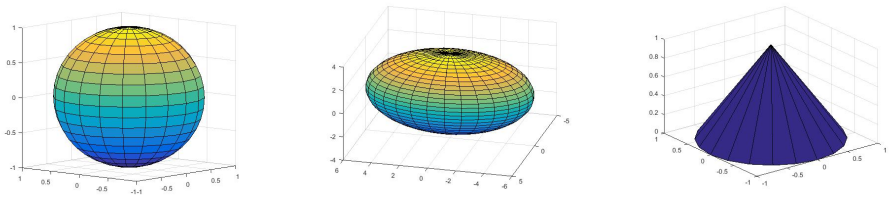

(a) $1 = x^2 + y^2 + z^2$ (b) $1 = \frac{x^2}{a^2} + \frac{y^2}{b^2} + \frac{z^2}{c^2}$ (c) $0 = \frac{x^2}{a^2} + \frac{y^2}{b^2} - \frac{z^2}{c^2}$

Figure 2.1: MATLAB plots of simple quadric surfaces.

We begin by defining a simple cylinder to depict a target. This is done by declaring the coefficients in Equation 2.1 corresponding to a cylinder centered along the y-axis with a radius of 0.9144 cm:

$$(1)\cdot z^2+(0)\cdot y^2+(1)\cdot z^2+(0)\cdot x\cdot y+(0)\cdot x\cdot z+(0)\cdot y\cdot z+(0)\cdot x+(0)\cdot y+(0)\cdot z = 0.83613 \tag{2.2}$$

As surfaces are infinite in extent, creating a finite subspace in the domain requires that the cylinder be delimited by two planes in the x-z plane. Subsequently, it is necessary to describe the logic expressions in the *Cells* card that tells the MC code where the region of interest lies. In other words, we must describe that we are interested in defining the region *inside* the cylinder. Using the Persistence of Vision Ray-tracer (POV-Ray) and 3D-RIBO (which converts the input file into a .pov file), the geometry can be rendered and checked for accuracy (Figure 2.2).

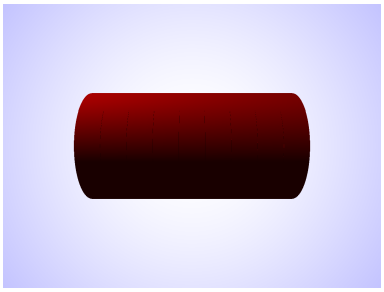

Figure 2.2: Ray-traced render of an empty target cylinder.

2.1.3 Adding foils

The target system that this work will focus on studying is a surface ion source (SIS). As mentioned in Chapter 1, the target is composed of many thin foils that are responsible for producing the radioisotopes of interest. As the arrangement of these foils is hypothesized to be responsible for the effusion release time, any simulation done on the system must accurately include these foils. The full

target specifications, as given by the TRIUMF Target Production E-LOG, are as follows:

- Total tantalum (Ta) foils = 470
- Foil thickness = 0.0025 cm
- Target density = 16.69 grams/cm^3
- Target length = 3.4 cm (exactly 7.8 cm space on both sides)
- Container length = 19 cm
- Total mass = 51.1533 grams (Including foils + Ta wire on 6 packs)

The total mass and density of the target are irrelevant for studying effusion and diffusion for foils constructed out of pure elements (for carbide targets, on the other hand, density is related to porosity which must be considered for both diffusion and effusion), as these parameters are only necessary to predict the production of isotopes, as discussed in Chapter 1. The container itself does not get defined in the input file as the particles are confined to the target volume once they are produced. Knowledge of its length merely gives us an upper bound on how long the target could conceivably be (say, by adding extra foils). RIBO formally understands only boolean intersections and cells are not defined by the union operation. The union operation is implicitly accounted for by cross-referencing cells that need to be connected. Therefore, if a surface shared by the container (should it have been defined) and the target is referenced both in the container cell and the target volume cell, these regions will be connected. That is, their union will be defined and particles will be allowed to move between them. If the thickness of the container were also to be defined, then this can lead to bizarre scenarios where particles are permitted to spend time flowing through solid tantalum.

Indeed, only the inner bore is required to be defined and defining the geometry should be an exercise in defining the 'inverse' of a SolidWorks model, for example. The space between physical objects is defined, not the physical objects themselves. Hence, anything the particles do not 'have knowledge of' need not be included in the input file. This is a necessary insight for defining the foils.

To begin with, 10 foils of thickness 0.0025 cm are added. These are defined implicitly by 'carving out' the existing, empty target. For n foils there will be $n-1$ spaces, and so 9 cells are defined using planes equally spaced by a distance of $(3.4 - 0.0025 \cdot 10)/9$ cm as depicted in Figure 2.3a.

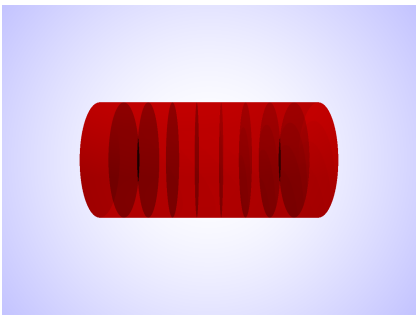

(a) 10 foils implicitly formed from segmenting the simple cylinder in Figure 2.2.

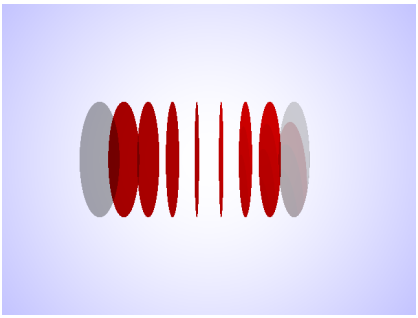

(b) Wireframe of 10 foils explicitly defined.

Figure 2.3: Simple target after adding interior foil structure.

However, the foils themselves are D-shaped to encourage effusive flow through the target. In order to implement this, a plane lying at the appropriate distance above the x-y plane is defined. The 9 void cells are then confined to live underneath this plane while a second cell to describe the void created above the plane is declared. They are cross-referenced to indicate to RIBO that these regions are connected, and that particles should be allowed to flow in between the foils and throughout the space above them. This adjustment is shown in Figure 2.4.

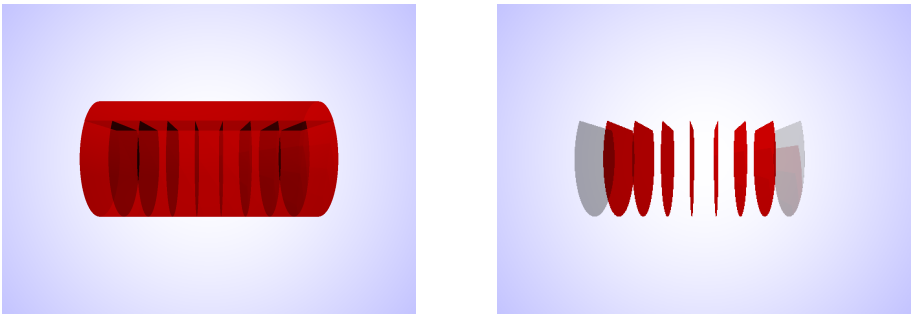

(a) (b)

Figure 2.4: D-shaped adjustment.

By the same procedure, this geometry can be generalized to any length or number of foils simply by generating a new list of plane positions and appropriately updating the index of the corresponding cells. An interactive program has been written for this purpose and enables rapid generation of new input files for TRIUMF's Target Module 3.

2.1.4 Full Geometry and Defining the Particle Source

In order to exactly represent the complex geometry of TRIUMF's target, an extended geometry was created. This was done by obtaining the specifications for the extraction tube and ionizer and adapting the RIBO depiction of the target (Figure 2.5b) from the model FLUKA geometry (Figure 2.5a). Two tubes were built, one with a 2.1 mm radius to act as the base of the extraction tube, and another with a 1.5 mm radius to represent the ionizer tube. In practice, a 10 mm by 10 mm rhenium foil is inserted into the end of the second tube as the 'ionizer'. This is represented by simply splitting the ionizer tube into two cells, where the second completes the end of the assembly and is delimited by two planes spaced 10 mm apart.

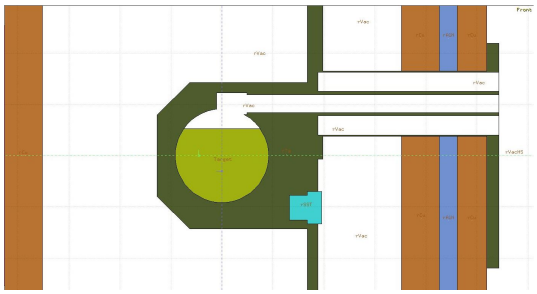

(a) Model FLUKA geometry.

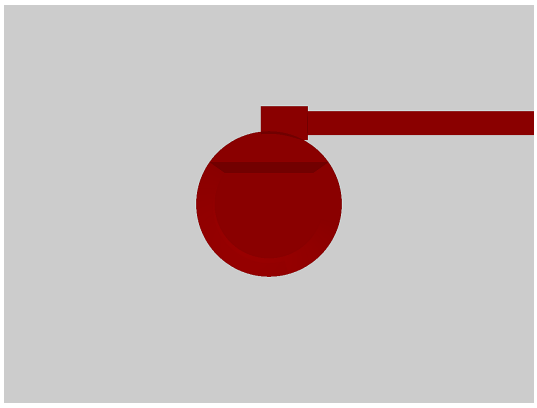

(b) RIBO depiction of target with extraction tube.

Figure 2.5: Target system representations

The 470 tantalum foils each with a thickness of 25μm are implemented by using the input file generation routine, as shown in Figure 2.6. As can be seen, the render poorly resolves the foils in the center of the target. POV-Ray builds an image by extending light rays into a scene, where they interact with a virtual object [14]. The rays are simulated according to classical laws, permitted to un-

dergo absorption, reflection, refraction or fluorescence. They are then recorded in an image plane and are rendered as .PNG or .JPG file.

However, due to the computational complexity of ray tracing 3D optical systems, if more reflecting objects are present in a scene the render time increases. Constraints on resolution are typically imposed to keep the CPU time and memory usage low. This is the cause of the aberration underneath the extraction tube observed in Figure 2.6.

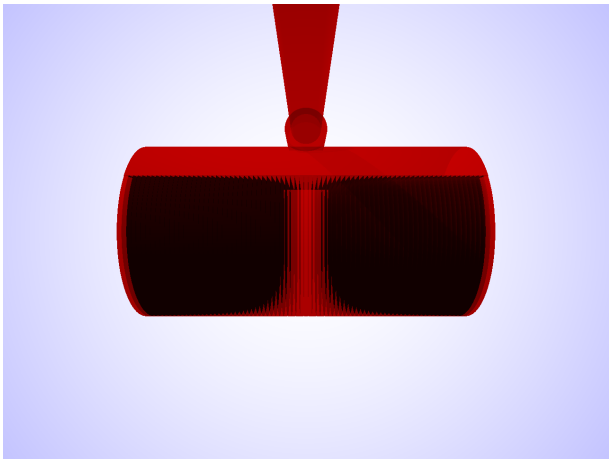

Figure 2.6: Ray-traced render of target with 470 foils and extraction tube. This image required 5.4MB of memory (peak), and took 6 minutes to complete. Note: the aberration in the middle of the target provides a misleading visual that there are no foils in the region under the extraction tube.

With the geometry complete, it is necessary to describe the source of the atoms to be simulated. The starting position and velocity coordinates are sampled inside a cylinder centered at the origin of radius 0.9144 cm and length 3.4 cm. The velocity of the particles is given by the atom temperature, as shown in Equation 2.3 (k_B is Boltzmann's constant, T is atom temperature, and m is the mass of one atom). It is assumed that the initial velocity of the atoms is equivalent to the temperature of the target, as the particles will have reached thermal equilibrium with the inner walls after several hundred collisions.

$$v_{rms} = \sqrt{\frac{3k_BT}{m}} \tag{2.3}$$

While a further analysis of the temperature dependence of an atom's behavior in the target is provided in the next section, for lithium, $m = 1.15 \cdot 10^{-26}$ kg, $T = 2300$K and so $v_{rms} = 2874$ m/s.

A first attempt at sampling particles in the target is shown in Figure 2.7. The starting trajectories of the atoms are allowed to be born anywhere throughout the target cylinder and no attention is provided to the nature of the interior

geometry. However, because the primary beam is non-rotating and has a diameter of 7 mm full width half maximum (FWHM), one would expect that the majority of particles should be produced where the foil 'sees' the beam. In this sense, a uniform cylindrical birth distribution is unlikely to be the true starting distribution (especially considering the foils are D-shaped, not circular). However, as the time it takes for a particle to travel the radius of a foil (in the void) is on the order of microseconds (much less than the half-life of even ^{11}Li), this is often a suitable approximation to make.

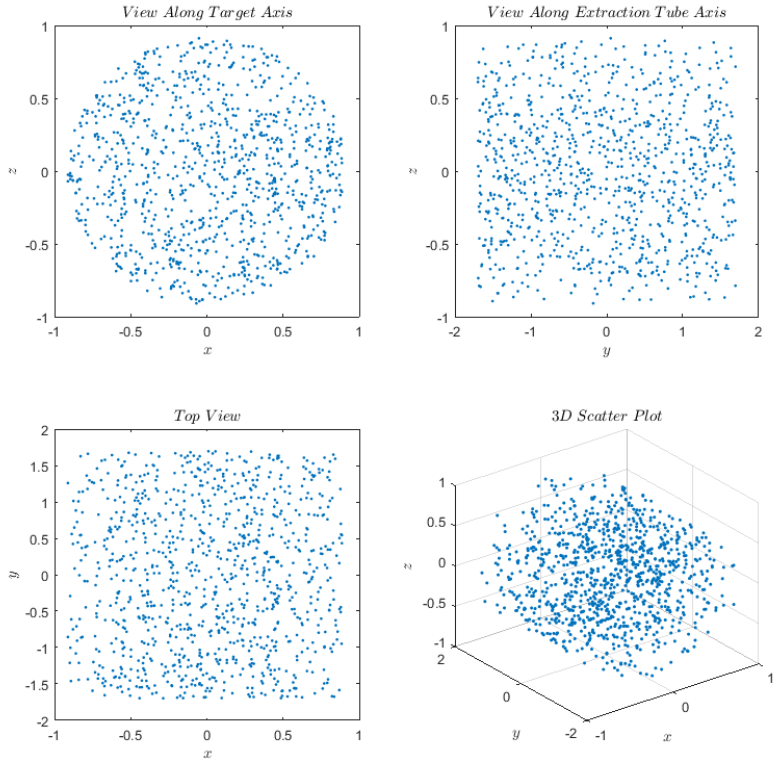

Figure 2.7: Plot group showing the starting coordinates of sampled particles in the xy, xz, and yz planes.

That said, it is possible to implement a more accurate source of particles. The first step requires eliminating the assumption that particles are allowed to be isotropically generated. Despite the symmetry of the target, there is a preferred particle production direction that's determined by the incident proton beam. To simulate the fact that the particles are produced along a central axis, the aperture of the particle distribution is set to zero to represent a focused beam. The central angle of emission is given to be the same as the axis of the target cylinder, $\hat{y}$ and 0.5 is set as the Gaussian radial dispersion of the birth distribution. At runtime, the source is limited to the foil cells and the output is shown in Figure 2.8.

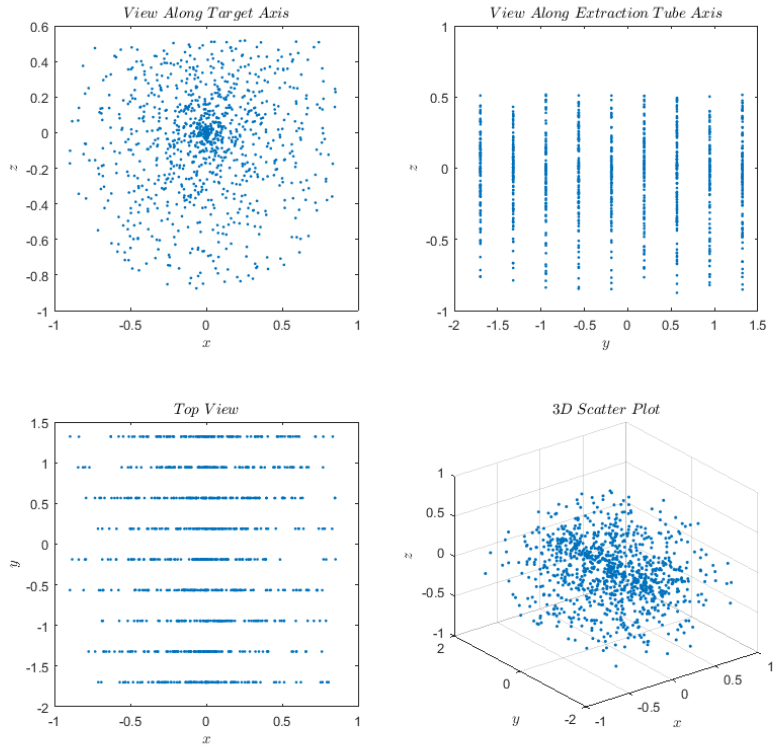

Figure 2.8: A more accurate description of particle birth coordinates in the target. The higher concentration of particles along the path of beam is visible, along with the D-shape of the foil and discrete birth lines corresponding to the individual foils. Note: the target simulated only contains 9 foils for comparative purposes. In the regime of 470 foils, these lines will be so close together that it would be indistinguishable from leaving the birth of particles unconstrained.

2.2 Temperature

It is important to recognize the temperature dependence of effusion and diffusion, considering that beam deposition dynamics produce a temperature gradient across the target (Figure 2.9). According to Equation 2.3, the speed of the effusing particles has a square root dependence on the temperature. Previous thermal simulations done at TRIUMF conclude that temperature across the target ranges from 2247-2611°C [3]. Table 2.1 shows what the corresponding spectrum of velocities are inside the target.

T (°C)	T (K)	v_{rms} (m/s)
2247	2520	3009
2450	2723	3127
2611	2884	3219

Table 2.1: Average particle velocities corresponding to target temperature for lithium.

This velocity spectrum ($\Delta v_{rms} = 210$ m/s) is implemented by matching the temperature gradient obtained from the solid target to each foil in the target.

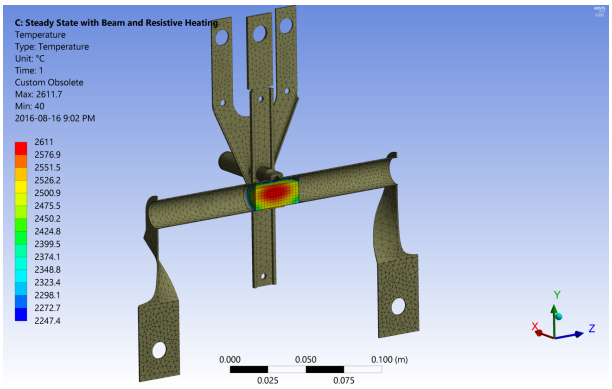

Figure 2.9: ANSYS simulation of a non-rotating proton beam impinging on the target. The temperature across the target ranges from 2247-2611°C. [3]

2.3 COMSOL Simulation for Non-uniform Diffusive Flux

For the study of isotopes diffusing through a single tantalum foil using the finite element method in COMSOL, the following assumptions have be made:

- Uniform temperature distribution across the foil.
- Semi-uniform initial concentration of isotopes.
- Diffusion coefficient of ^{8}Li is similar to ^{7}Li.
- Time-dependent.
- No convection.
- In-target production is symmetric and centered within the foil.

The geometry of the simulation is very simple. To create the foil, we start with a single cylinder with radius 0.9144 cm and thickness 0.000125 cm (half of the foil). Next, a second cylinder of radius 0.35 cm is superimposed on the existing surface. This will enable the delimiting of the initial concentration of diffusing species according to the nature of the beam intensity (7 mm FWHM). A third cylinder is superimposed with a radius of 0.7 cm to emulate the tails of the beam where the concentration is taken to be $0.5C_0/e$. Finally, a block centered at 1.05 cm is superimposed on the existing domains and, using the Boolean Difference function, the region is subtracted to yield the D-shaped foil.

Under the materials section, solid tantalum and lithium gas are added. The former is applied to the entire body and the latter is selected as the diffusing species. Under the Chemical Species Transport physics tab, "Transport of Diluted Species (tds) is selected and the diffusion coefficient is selected to be $0.9{\cdot}10^{-8}$(Li, Ta, 2423 K) [12]. Initial values are set to 0 mol/m^3 and two concentrations are applied to the regions mentioned above. For the center of the foil, a concentration of 0.003 mol/m^3 was chosen in place of reliable data and for visualization purposes. The annular region used to model the tail of the beam is set to be 18% of this maximum concentration. This crude representation of the beam's Gaussian spread is simply to prove that such modeling can be done. A more accurate representation of the concentration gradient can be implemented using the same method if desired, however this would entail a fairly laborious process of manually calculating and assigning concentrations. In this case, it would be worth investigating if COMSOL has a built-in feature to automatically define a Gaussian concentration gradient across a surface.

As it is assumed that the radioactive nuclei are birthed in the center of the foil and diffuse symmetrically outward to the front and back surface, only half of the foil is simulated. Due to the extremely thin nature of the component, a very fine mesh is required to ensure that the element size is smaller than the edge of the foil thickness. A further simplification could be made to investigate only a quarter of the foil as symmetry would still hold. This may be required if future, more detailed simulations turn out to be time-intensive.

2.4 Surface Ionization

In order to simulate the ionization and transport of ionic species, the surface ionization program (surfION.f) must be activated in RIBO. The requires knowledge of the ionizing surfaces and cells which they belong to, the atomic numbers of the effusing species (Z = 3, for lithium) and substrate (Z = 75, for rhenium). As mentioned in Section 2.1, the ionizing cell is set to be the last 10 mm segment of the extraction tube. After each collision a particle suffers with an ionizing surface, it will have a probability of being ionized given by Equation 1.7. The events that exit the target in an ionic state are tallied and can be analyzed outside of the program.

2.5 Data Output and Analysis

The simulation returns data in a tab-delimited ASCII file that contains a tremendous amount of information. Each line of the output file contains the ionic state (denoted as a 1 for ions, and 0 for neutrals), the birth coordinates, diffusion time in bulk, number of collisions, flight time in the void, and the effusion/diffusion

time per particle. In order to efficiently analyze the results, the ASCII file is passed to a MATLAB script.

This script reads the file, makes plots of the starting distribution of the particles, calculates the total release time by multiplying a user-defined sticking time by the number of collisions and adding it to the flight time of each particle, populates histograms of ions and neutrals, plots the statistical fit provided by RIBO, plots particle trajectories, and computes release fractions. The average figures associated with each simulation can be extracted manually and entered into a spreadsheet for further analysis.

To ensure the accuracy of the results, each simulation is run 5 times using the same number of histories and runtime conditions. The error in each of the parameters of interest for these runs is calculated by Equation 2.4

$$\% \; Error = \frac{\sigma}{\frac{1}{5}\sum_{i=1}^{5} X_i} \times 100, \tag{2.4}$$

where X_i is the parameter of interest (average release time, for example) for the i^{th} run and σ is the standard deviation between the runs. This is also known as the Coefficient of Variation and is used in statistics to interpret the relative magnitude of the standard deviation in the simulation results. However, it does not account for systematic errors.

3 Results

The methodology for conducting simulations of the TRIUMF target system has been developed in Chapter 3. A study of the release times and release efficiencies of short-lived isotopes is now carried out in order to identify optimal configurations for future targets. The analysis provides an explanation for how targets should be designed to account for the isotope-dependent processes. As no previous RIBO simulations had been conducted at TRIUMF before, tests are run against literature values to ensure that the simulation setup was operating as expected.

3.1 The SPES Target

In order to become validate the RIBO distribution provided to TRIUMF, the geometry and target operating conditions were first replicated from M. Barbui's 2007 paper "Release time calculations for the SPES direct UCx target" [24]. The SPES (Selective Production of Exotic Species) Project at Legnaro National Laboratories (LNL), one of the four national labs of the Italian Institute of Nuclear Physics (INFN), houses a target used for the production of neutron-rich radio-active nuclei. It is a fission-based ISOL system that uses a 40 MeV, 0.2 mA primary proton beam to drive a high number of nuclear fission reactions in uranium carbide disks. The target disk material is porous and, for this reason, the movement of particles in the powder can be modeled with effusive-flow, and the flow in the void can be modeled using traditional effusion. A major component of the project was a study of the release of radioactive isotopes from the disks to the ion source. Using RIBO and GEANT4, a physics simulation toolkit, an estimation for the release time of neutron-rich nuclei was performed by Barbui. The availability of existing release time calculation results coupled with an in depth discussion of the setup of the study provided a good departure point for this work.

In the paper, it is assumed the the SPES UC_x disks comply with the standard ISOLDE parameters [25], which means the average flight path in the UC_x powder is 15 μm and the sticking time is 10^{-6} seconds.

The specifications for the target, as listed on the SPES Project website, are as follows:

- Target disk diameter: 3 cm
- Disk thickness: 0.9 - 1.3 mm
- Disk density: 2.5 grams/cm^3
- Spacing: 2 cm
- Number of disks: 7
- Operating temperature: 2273 K
- Exit cone radius: 0.4 cm
- Container diameter: 4 cm
- Total length: 24 cm

The combinatorial geometry for this target is adapted from an existing input file provided with RIBO. It comprises 28 surfaces, 14 cells/regions and a source card containing the reference particle Krypton-90 (^{90}Kr). Figure 3.1 is the 3D render.

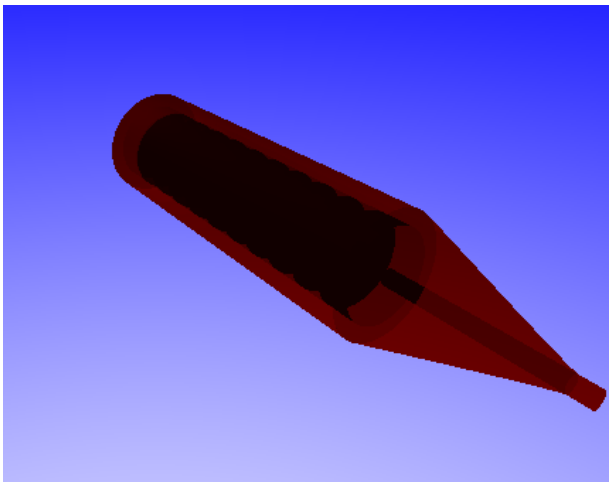

Figure 3.1: SPES target model.

A simulation of 5,000 histories is run and the results for the average number of collisions, ⟨Coll⟩, and path length, ⟨Path⟩, inside the target volume are presented in Table 3.1. The total average effusion delay time was reported to be 0.22 ± 0.02 seconds, which agrees perfectly with the recorded literature value referenced in Table 3.1 [24]. This indicates that even with a simulation of 5,000 histories, the statistics are decent.

	M. Barbui	Benchmark Simulation
$\langle$Coll$\rangle$	4034 $\pm$ 292	4177 $\pm$ 290
$\langle$Path$\rangle$	159 $\pm$ 10 m	160 $\pm$ 10 m
$\langle t_{eff} \rangle$	0.22 $\pm$ 0.02 s	0.22 $\pm$ 0.02 s

Table 3.1: Comparison between literature values and benchmark simulation of effusion in vacuum (excluding powder).

To gain an understanding of how the nuclei effuse through the target, the trajectory of a single particle is simulated. The position as a function of time is then plotted using the MATLAB analysis script as shown in Figure 3.2. The birth of the particle is selected to be the third pill from the extraction tube and it is easily visible that the particle spends most of its time navigating through the back of the target before exiting after 433 collisions. It takes 0.02196 seconds to complete its average free path of 15.7379 meters. If a particle is simulated closer to the back of the target (in the pill furthest from the extraction tube), it takes 0.6449 seconds after 11906 collisions to make it to the exit hole. Therefore, in this configuration short-lived isotopes produced at towards the back of the target are unlikely to survive long enough to get extracted.

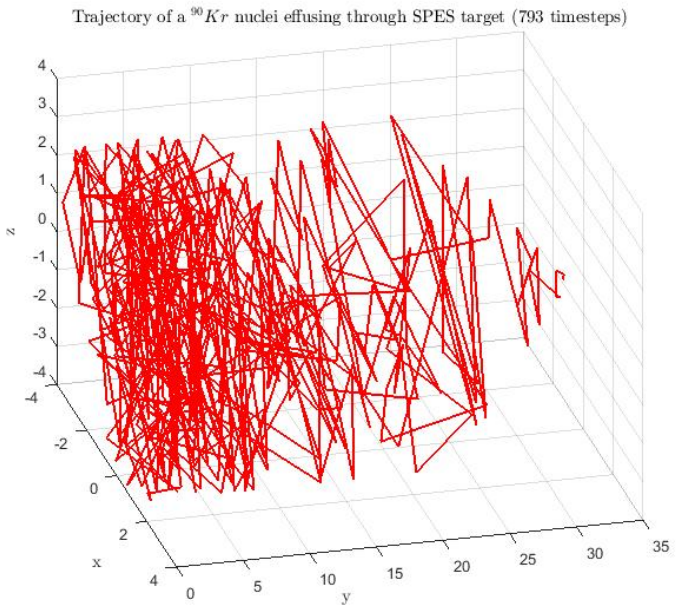

Figure 3.2: Trajectory of a particle migrating through the SPES target model shown in Figure 3.1.

For ^{90}Kr, with a half-life of 32.32 seconds, it is expected that the majority of produced isotopes will make it to the exit before decaying. The effusion release curve is plotted in Figure 3.3. Following the discussion in Section 1.1.2, the

effusion release efficiency can be calculated by Equation 3.1:

$$\epsilon_R = \int_0^\infty E(t) \cdot exp\Big(- \frac{t^i \cdot ln(2)}{T_{1/2}} \Big) \cdot dt \tag{3.1}$$

where t^i is the individual total release time, $T_{1/2}$ is the half-life of the species and $E(t)$ is the intrinsic release function for effusion. Calculating this value for ^{90}Kr yields a value of 80%.

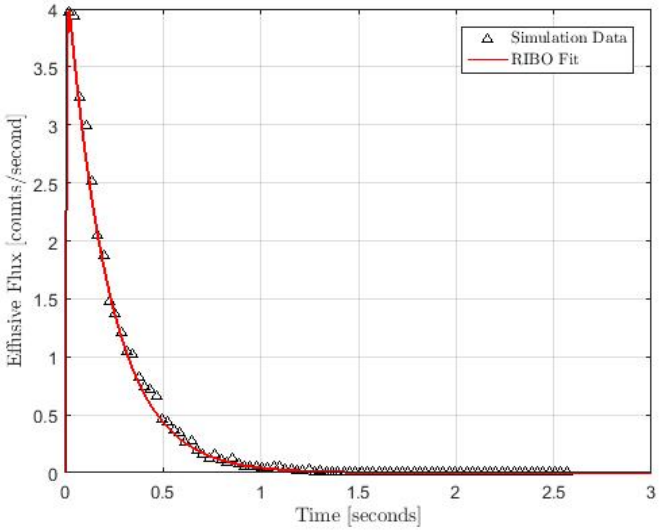

Figure 3.3: A plot of $E(t)$ fit to simulation data of ^{90}Kr release from the SPES target.

A similar procedure is now followed for the TRIUMF target system, where an in depth analysis of the simulation results is provided.

3.2 TRIUMF's Target System

The reference particle chosen for the simulations is ^{11}Li as it is the heaviest and hence slowest (by Equation 2.3) of the lithium isotopes. Regardless, the release times of other isotopes can be scaled down to the square root of the isotope mass in question (by using the factor $\sqrt{\frac{mass\ of\ species\ ^iX}{mass\ of\ ^{11}Li}}$). The results for the flight time of one isotope can be scaled up or down to any other isotope, removing the need for running multiple time-consuming simulations.

A trace of the trajectory of a single isotope effusing through the target geometry is shown in Figures 3.5 and 3.6 and yields some striking results.

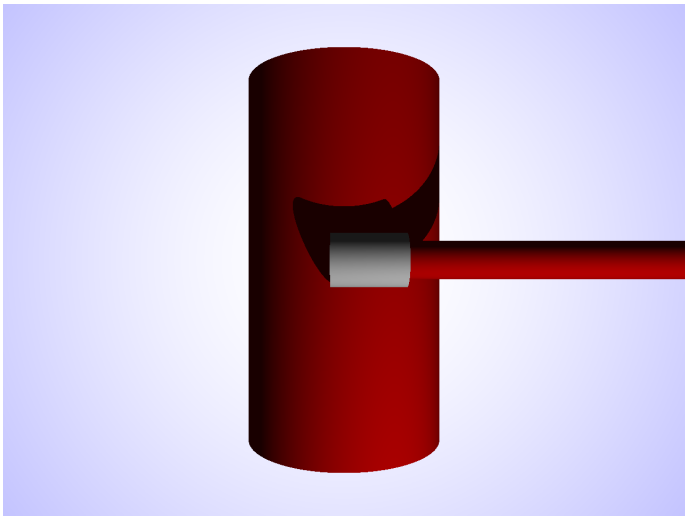

Figure 3.4: Top down view of TRIUMF target.

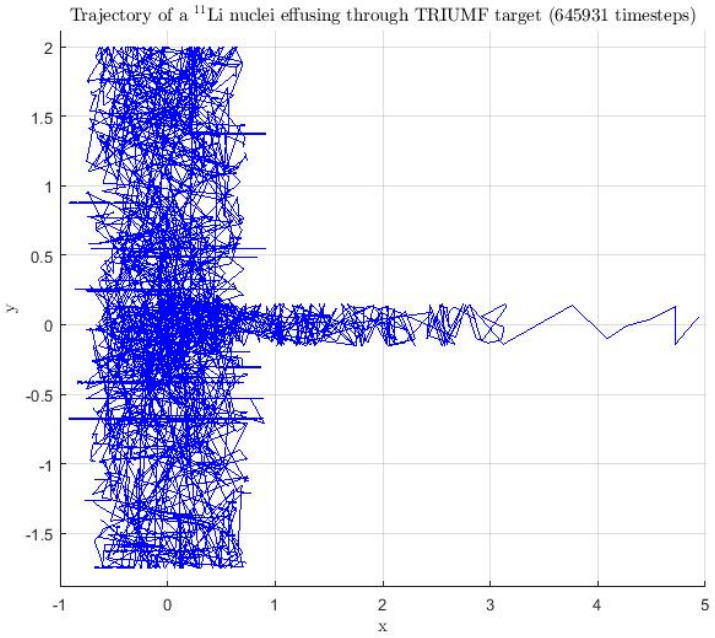

Figure 3.5: A plot of a single ^{11}Li particle effusing through geometry with just over 470 foils. Note: view is from the top down.

The particle was produced roughly in the center of the target and follows a non-trivial trajectory to the ionizer after 0.037 seconds, suffering 645,931 collisions with an average free path of 77.7 m. In this particular target, the distance between the foils is set to be a fixed length of 0.0047 cm. This value corresponds to the foil spacing for a tightly packed target and is calculated from the target specifications provided in Section 2.1.3.

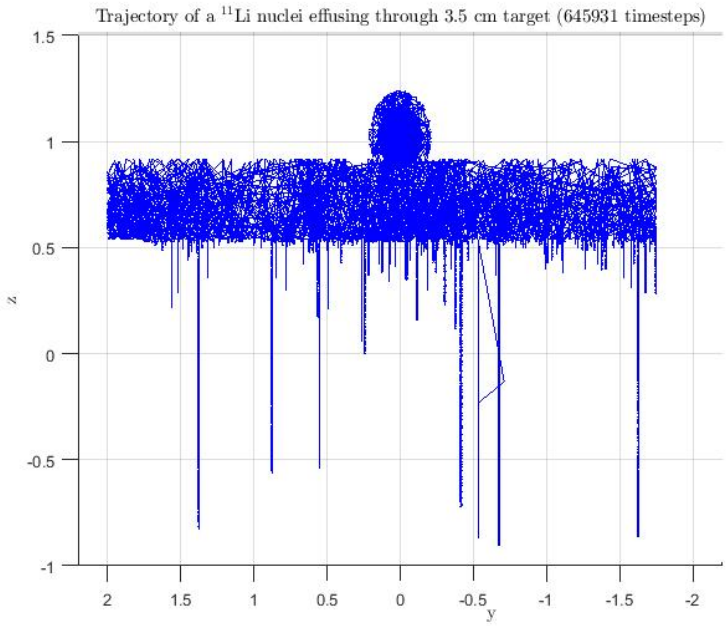

Figure 3.6: A plot of a single ^{11}Li particle effusing through geometry. Note: view is from the back of the target. The 'drip-lines' observed below $z = 0.5$ show the particle entering the space between foils (region defined on $-1 < z < 0.5$) many times before finally exiting the geometry. The region $0.5 < z < 1$ corresponds to the void above the foils. The particle experiences nearly 650,000 collisions before exiting the ionizer tube.

The true number of foils in this model is 484, which corresponds to a target length of 3.5 cm. Though this is 0.1 cm longer than a target containing 470 foils, it was chosen to make the implementation of the simulation arrays more straightforward. An analysis of the average effusion time in each cell indicates that out of the 483 spaces between the foils, only 15% are not explored by the particle. The tallest peak in Figure 3.7 corresponds to the cell representing the void above the foils. It makes sense that the particle will spend the most time here, as it must travel further between successive collisions before it can eventually escape. There are 22 cells that have peaks greater than 1% and these can be seen in Cartesian coordinates as the 'drip-lines' in Figure 3.6. In fact, 95% of the cells have a time-share less than 1% meaning that, while a particle could get trapped in a void between foils for some time, the main delaying mechanism in this geometry is the void above the D-shaped foils. However, this discussion only concerns one particle. Computing the average figures for a simulation of 1,000 particles shows that the time spent between the foils is negligible compared with the time spent in the void above them and in the extraction tube with 99% of the cells having a time-share less than 1%.

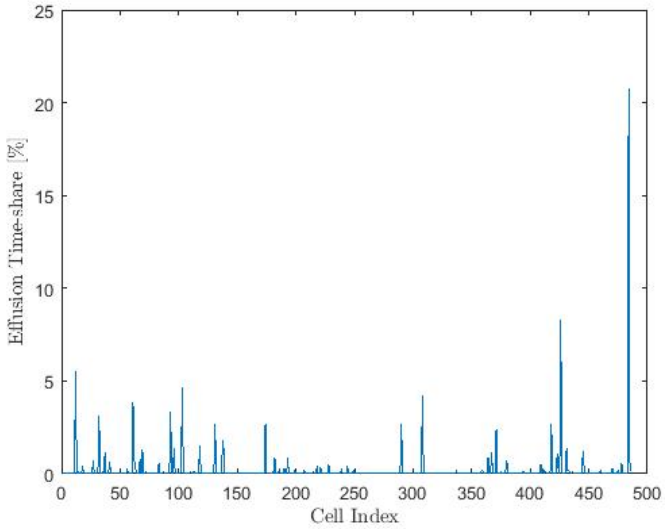

Figure 3.7: Effusion time-share in each cell for a single particle. The sharp peak near cell index = 500 corresponds to the void directly above the foils.

3.2.1 Release Curve and Efficiency Calculations

The individual delay times for each history is stored in a histogram of equal bin width (Figure 3.8). A double-exponential function is used for the effusion release curve, $E(t)$, to model the fast rise and decay of particles exiting the ionizer [31].

$$E(t) = C(1 - e^{-t/t_1})e^{-t/t_2} \tag{3.2}$$

Equation 3.2 is obtained from the statistical analysis conducted by RIBO and normalized to the distribution by toggling the fit parameter C. This analytic function describes the release distribution probability and the parameters t_1 and t_2 are provided in the output file. However, these parameters are calculated assuming a uniform bin size. If a custom, variable bin width was used to resolve the detail of the fast rise of the distribution, the parameters would no longer be valid and a least-squares fit would have to be performed to the distribution [29]. Though this may be useful for visualization purposes, such a procedure would have no influence on the efficiency calculations so long as the distribution function remains normalized. In order to take full advantage of the conveniences afforded by RIBO, all analysis is performed using a uniform bin width.

The reason why it's important to obtain the intrinsic release curve, $E(t)$, is so that it can be ultimately convoluted with the decay law of a given isotope to obtain the overall effusion efficiency, ϵ_{eff}, for a given isotope. The diffusion function can be treated analytically, numerically or by sampling diffusion times

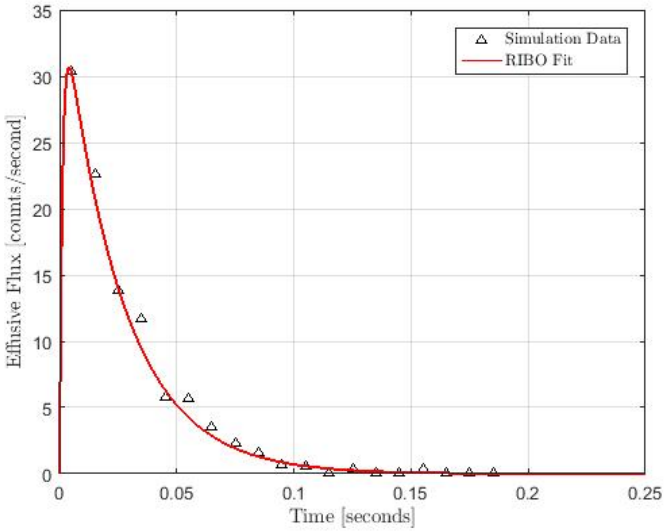

Figure 3.8: A plot of $E(t)$ fit to simulation data of lithium release from the TRIUMF target. The fit parameters are: $C = 38(\pm 2\%)$, $t_1 = 0.00137(\pm 3.993\%)$, $t_2 = 0.02511(\pm 4.394\%)$.

from a probability distribution. By the same method, the diffusion efficiency can be obtained by convolving the diffusion profile with the associated decay law, as will be presented in Section 3.2.2. The effusion release efficiency is obtained by evaluating Equation 3.1 for the half-lives of interest (Table 3.2).

Isotope	Half-life (ms)
^{8}Li	840.3(9)
^{9}Li	178.3(4)
^{11}Li	8.75(14)

Table 3.2: Half-lives of several isotopes of lithium [15].

Figure 3.9 displays the convoluted release functions for effusion. For ^{7}Li, the release fraction is calculated to be equal to unity. This makes sense, as ^{7}Li is stable and so it is expected that 100% of the produced nuclei will make it to the exit of the ionizer. On the other hand, it is shown that the release fractions of ^{8}Li, ^{9}Li, and ^{11}Li decrease correspondingly with half-life.

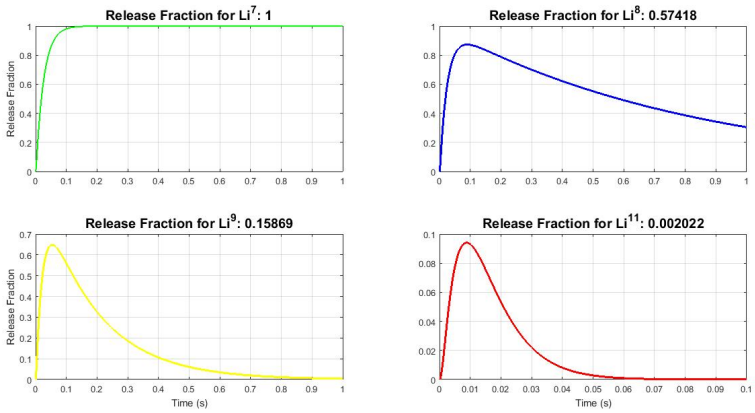

Figure 3.9: Plots of the effusion release curves of ^{7}Li, ^{8}Li, ^{9}Li, and ^{11}Li. The associated effusion release fraction, ϵ_{eff}, is calculated to be 100%, 58%, 16% and 0.2%, respectively.

Diffusion Efficiency

The diffusive flux of particles out of a foil as a function of time depends on the foil thickness [13]. As such, if the thickness of the foil is held constant there is not much that can be done to improve the diffusion release efficiency other than increasing the temperature of the target. However, the maximum temperature that a target can operate at is constrained by the melting temperature of tantalum (3,020°C) [28]. Using RIBO to sample diffusion times for a variety of foil thicknesses, it is possible to gain insight into how the diffusion efficiency of a particular isotope depends on the foil thickness (Table 3.3). To calculate these values, a similar procedure is followed for the effusion efficiency by integrating the function

$$\epsilon_{diff} = \int_0^\infty DF(t) \cdot exp\Big(- \frac{t^i \cdot ln(2)}{T_{1/2}} \Big) \cdot dt \tag{3.3}$$

where the diffusive flux is given by Equation 3.4 for the statistical fit parameter t_D [23], [12].

$$DF(t) = \frac{exp(-t/t_D)}{t_D} \tag{3.4}$$

Figure 3.10 displays the release curves for the diffusive flux of lithium out of several foil thicknesses. It can be seen that the average diffusion release time for the 25μm foil, which is the thickness chosen for the TRIUMF target this study concerns, is 26.1±3.9 seconds. Considering the half-life of the lithium isotopes of interest are on the order of tens to hundreds of microseconds, considerable losses from diffusion should be expected.

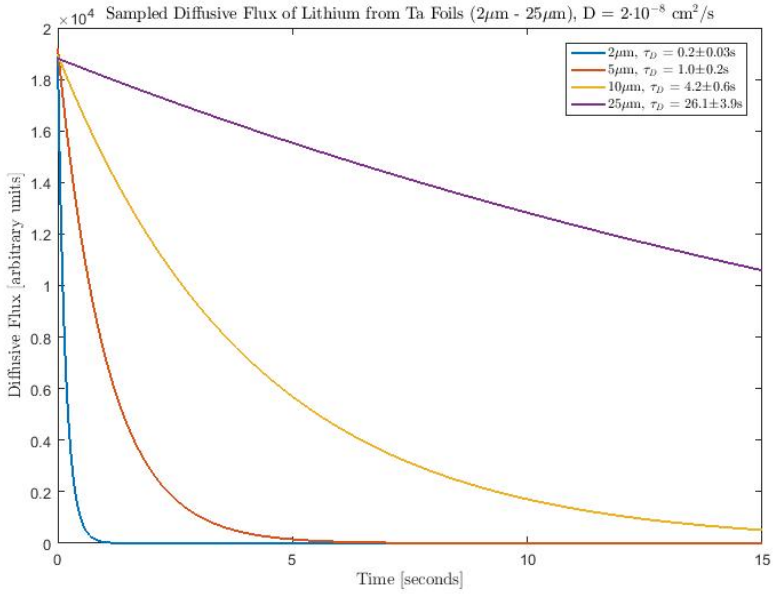

Figure 3.10: Plots of the diffusion release curves for foil thicknesses 2μm, 5μm, 10μm, and 25μm. The average diffusion release time, τ_D, for these thicknesses is 0.2±0.03 seconds, 1.0±0.2 seconds, 4.2±0.6 seconds, and 26.1±3.9 seconds, respectively.

d (μm)	^{7}Li	^{8}Li	^{9}Li	^{11}Li
2	100%	64.1%	18.1%	0.12%
5	100%	60.1%	13.2%	0.042%
10	100%	59.2%	12.2%	0.034%
25	100%	58.9%	11.9%	0.032%

Table 3.3: Diffusion release efficiency, ϵ_{diff}, for several lithium isotopes as a function of foil thickness, d.

It can be seen that the diffusion efficiency of ^{11}Li decreases by an order of magnitude as the foil thickness is increased from 2μm to 5μm whereas the efficiencies for ^{8}Li and ^{9}Li decrease by a couple of percent, at most. Therefore, thinner foils are the best choice for improving the diffusion efficiency. However, using thinner foils corresponds to less material to produce the isotopes in the first place which would lower the production efficiency of the isotopes [27]. While it would be feasible to address this by simply increasing the length of the target (by adding more foils), this is suspected to have an antagonistic effect on the release time and should be investigated.

3.2.2 Influence of Target Length and Foil Number

If thinner foils are chosen and targets lengthened accordingly to account for decreased production, it would be useful to be able to predict the effect this might have on the release time. A simulation array was run for a variety of

target lengths keeping the distance between the foils constant. As shown in Figure 3.11, it is found that the average release time increases linearly with target length. It is important to acknowledge that the average release time for the longest target simulated (8.5 cm) is still less than the half-life of ^{8}Li and ^{9}Li. This suggests that the effusion efficiencies for these isotopes should not change drastically, however, there should be a noticeable decrease in ^{11}Li as target length is increased.

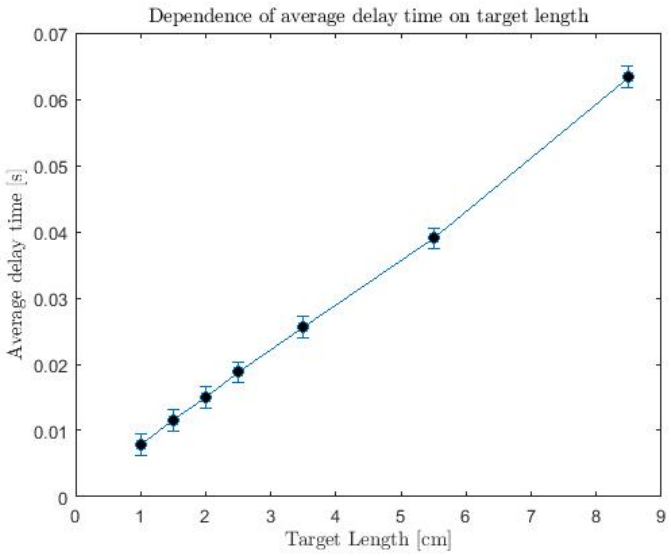

Figure 3.11: Dependence of average delay time on target length.

In order to validate this, the effusion profiles are plotted in Figure 3.12 and effusion release fractions calculated in Table 3.4. Indeed, it is shown that while the release of ^{8}Li and ^{9}Li decrease by only 1-3%, the ^{11}Li release decreases by several factors.

Length (cm)	^{7}Li	^{8}Li	^{9}Li	^{11}Li
1.5	100%	67.7%	24.4%	0.659%
3.5	100%	67.3%	23.4%	0.393%
5.5	100%	66.9%	22.7%	0.296%
8.5	100%	66.2%	21.4%	0.198%

Table 3.4: Effusion efficiency as a function of increased target length.

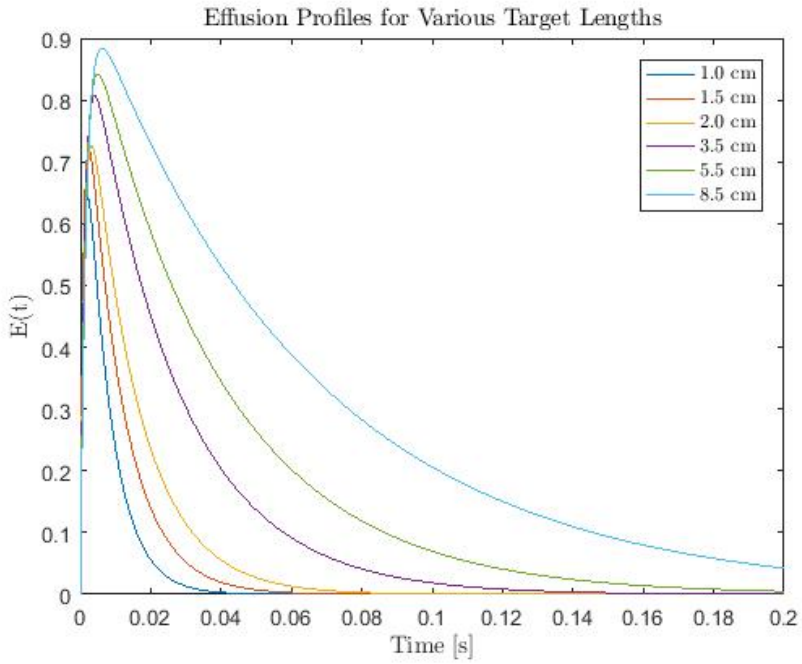

Figure 3.12: Effusion profiles for target lengths 1.0 cm, 1.5 cm, 2.0 cm, 3.5 cm, 5.5 cm, and 8.5 cm.

3.2.3 Additional Dependencies

Another parameter that is possible to tune is the foil spacing, which would give insight into how tightly the foils should be packed in order to maximize the release. A series of simulations are run where the target length is held constant (3.5 cm) and the number of foils increased from 10 to 400. Figure 3.13 shows that as the number of foils is increased, the average delay time decreases by approximately 20%. This suggests that as the foils are packed more tightly, the spacing between the foils will decrease and hence the average distance between collisions suffered by a particle should also decrease resulting in a shorter path on average for the particles to travel (Table 3.5). The correspondence between number of foils and average distance between collisions is shown in Figure 3.14.

Number of Foils	Mean Free Path (m)
10	68.8
20	68.9
40	67.9
80	66.3
200	59.9
400	54.3

Table 3.5: Mean-free path travels by a particle from birth to exit. Note: the slight increase recorded from 10 to 20 foils is a statistical anomaly. As only one simulation was run to obtain these values, no error bars could be added.

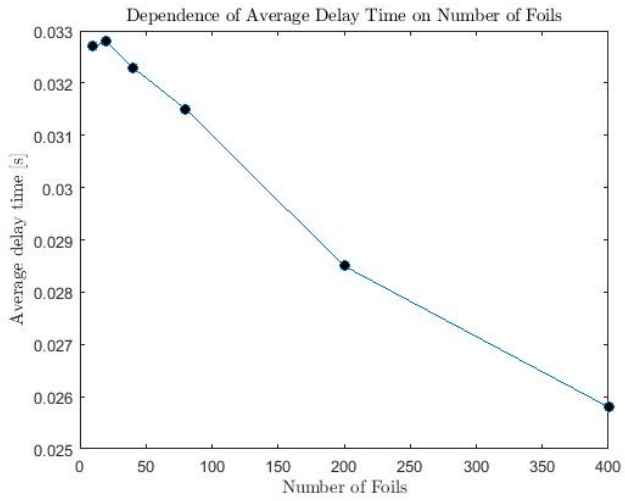

Figure 3.13: Dependence of average delay time on number of foils (fixed target length).

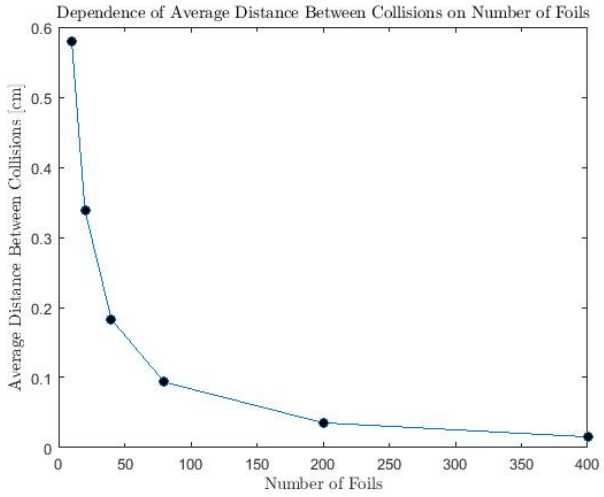

Figure 3.14: Dependence of average distance between collisions on number of foils.

The reason for the absence of error bars in these simulations is due to the computation time of simulating increasingly complex geometries (Figure 3.17). While the simulation of 400 foils confined to a 3.5 cm long target took 2 hours for 1,000 histories, the simulation of an 8.5 cm long target containing 1174 foils took close to 17 hours for 1,000 histories (the entire simulation array took 30 hours to complete). While it is possible to run the array as a background operation on a computer (or even distribute it across multiple processors), running one simulation as a quick scan should suffice to gain an understand of the expected trends.

The influence of sticking time, t_s, is also investigated. Figure 3.15 shows that as t_s increases beyond 1×10^{-8} seconds, the average effusion time begins to increase. This suggests that for isotopes with large t_s, tightly packed foils can actually hinder the release. For lithium isotopes, where the sticking time is on the order of nanoseconds, the tightly packed foil configuration is still advantageous [16].

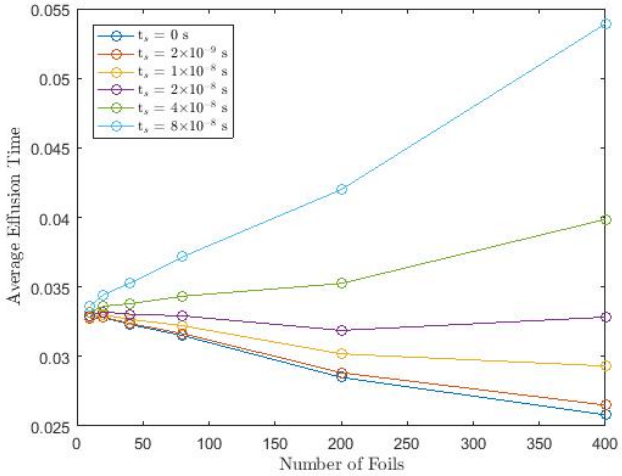

Figure 3.15: Relationship between increased sticking time and average effusion time. It can be seen that the effusion time begins to diverge with an increased number of collisions, recalling that the total effusion time taking into account sticking is calculated by $t_{eff} + t_s \cdot N_{collisions}$. The number of collisions scales with foil number as shown in Figure 3.16

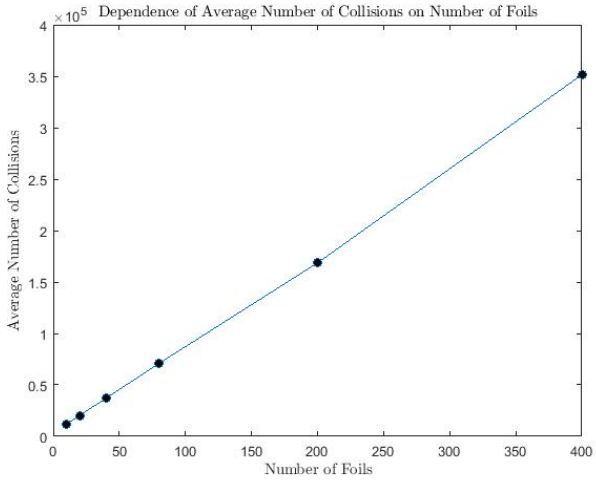

Figure 3.16: Average number of collisions as a function of number of foils in a fixed length target.

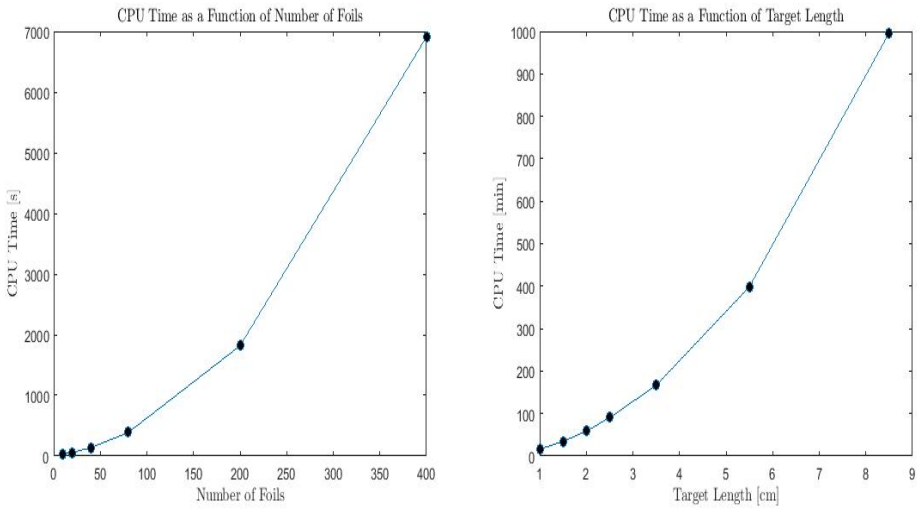

Figure 3.17: Exponential increase in CPU time plotted as a function of number of foils and target length.

3.2.4 Ionizer Surface Area

As this point, it should be acknowledged that while this study has delved into the behavior of the target's geometry, that ionizer tube length and radius also has an influence on the release properties of the target [18]. In particular, the ionization efficiency and the effusion efficiency vary inversely with a decrease in the aspect ratio of the ionizer tube and the corresponding absolute extraction efficiencies have been characterized in previous literature [12]. As the influence of ionizer surface area on ionization efficiency has not yet been investigated, Table 3.6 summarizes the results of a series of simulations where the presence of the rhenium ionizing material is increased. It appears that increasing the length of the region where ionizations can occur decreases the efficiency. This could be attributed to the fact that more collisions with an ionizing surface also increases the chance of recombination and hence the probability that an atom will exit as a neutral.

Length (cm)	Surface Area (cm^2)	Ionization Efficiency (%)
1	1.07	21.9($\pm$1.3)
2	2.01	21.2($\pm$1.3)
3	2.94	18.7($\pm$1.1)
4	3.87	17.2($\pm$1.2)

Table 3.6: Ionization efficiency, ϵ_i[%]($\pm$ relative error), of lithium as a function of rhenium surface area for the TRIUMF ionizer tube (radius of 1.5 mm and length 4.5 cm). The temperature of the ionizer is set to 2300K.

3.2.5 Emittance

In addition to ionization, RIBO permits the study of beam shape as particles exit the ionizer. This is known as beam emittance and is a measure of the divergence of the beam. Instead of providing information about the spatial distribution of particles at the end of the ionizer, the emittance provides spatial and velocity information. Figure 3.18 is a plot of the emittance map in a plane (z, y) transverse to the extraction axis $(\hat{y})$. The y-axis plots the velocity divergence, $\alpha_{z,y}$, and the x-axis plots the position, dz.

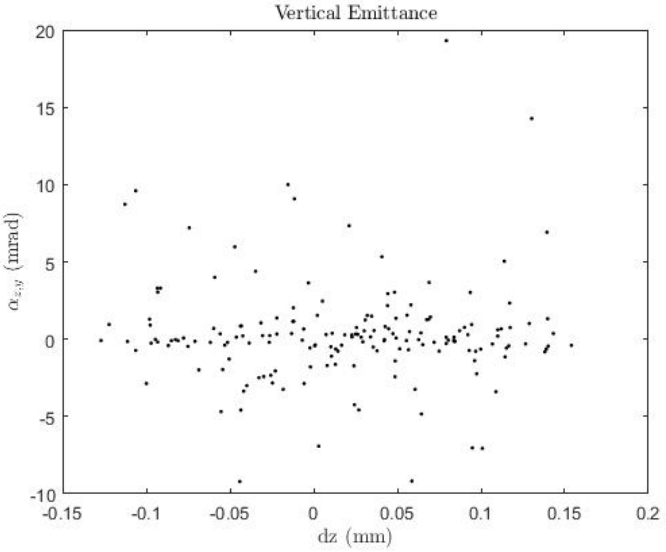

Figure 3.18: Output of the emittance map produced by RIBO.

4 Future Work and Conclusions

4.1 Outlook

Further simulations may be carried out to investigate how different foil shapes influence the release times. In particular, annular and circular foils could be studied. Carbide targets could also be simulated in order to obtain results than can be compared to the experimental data available for francium isotopes $^{211-214}$Fr. RIBO also permits the defining of electromagnetic fields which could be implemented to match the TRIUMF extraction system. Furthermore, the design of the ionizer exit hole could be changed to probe the effects on emittance. Indeed, beam emittance is a key link to accelerator physics and should be given much more attention in future studies. TRIUMF also employs other ionization processes (such as resonant laser and electron impact) that could be included in future simulations. Lastly, these studies could be carried out for a wider range of isotopes in use at TRIUMF.

4.2 Summary

A simulation of radioactive isotope release has been performed for the TRIUMF target system using RIBO. The ionization, effusion and diffusion efficiencies have been examined for several target configurations for ^{8}Li, ^{9}Li, and ^{11}Li isotopes, providing insight into how optimal configurations could be developed. A comprehensive overview of setting up RIBO simulations has been provided and a set of codes for producing input files and conducting the data analysis of output files is included in Appendix A. As a function of half-life, it is found that shorter targets are more useful when very short-lived isotopes are desired. The diffusion efficiency analysis suggests that targets with varying thicknesses (thin near the ionizer to allow for quick release of very short-lived species) may also be beneficial.

References

[1] Rummukainen, Kari. Monte Carlo Simulations in Physics. N.d. Notes. Department of Physical Sciences, University of Oulu.

[2] Bricault, P. "High Power Targetry for ISOL Facilities." 5th High Power Targetry Workshop, FermiLab (2014): n. pag. Web. Nov. 2016.

[3] Courtesy of Y. Beilouni and A. Laxdal, 2016.

[4] "The FLUKA Code: Developments and Challenges for High Energy and Medical Applications" T.T. Bhlen, F. Cerutti, M.P.W. Chin, A. Fass, A. Ferrari, P.G. Ortega, A. Mairani, P.R. Sala, G. Smirnov and V. Vlachoudis, Nuclear Data Sheets 120, 211-214 (2014)

[5] Garcia, Fatima H. "Calculation of Rates for Radioactive Isotope Beam Production at TRIUMF." Thesis. Simon Fraser University, 2016. Print.

[6] "FLUKA: a multi-particle transport code" A. Ferrari, P.R. Sala, A. Fasso, and J. Ranft, CERN-2005-10 (2005), $INFN/TC_05/11$, SLAC-R-773

[7] Crank, John. The Mathematics of Diffusion. Oxford: Clarendon, 1979. Print.

[8] Fujioka, M., and Y. Arai. "Diffusion of Radioisotopes from Solids in the Form of Foils, Fibers and Particles." Nuclear Instruments and Methods In Physics Research 186.1 (1981): 409-12. Web.

[9] Leitner, Mario Santan. RADIOACTIVE ION BEAM OPTIMISER, RIBO. USER MANUAL. N.p.: n.p., 2005. Print.

[10] MATLAB. Computer software. Vers. R2016b. The MathWorks Inc., n.d. Web. ¡https://www.mathworks.com/products/matlab.html¿.

[11] Giesler, Gregg C. MCNP Software Quality: Then and Now. Proc. of 10th International Conference on Software Quality, New Orleans, Louisiana. N.p.: n.p., 2000. Print.

[12] Leitner, M.S. (2005) "A monte carlo code to optimize the production of radioactive ion beams by the isol technique" (Doctoral dissertation). Retrieved from http://cds.cern.ch/record/905537/files/thesis-2005-039.pdf?subformat=pdfa/version=2

[13] Bennett, J. R.J. "The Development of Fast Tantalum Foil Targets for Short-lived Isotopes." Beam Interactions with Materials and Atoms (2005): 215-19. Www.elsevier.com/locate/nimb.

[14] Persistence of Vision Pty. Ltd. (2004), Persistence of Vision Raytracer (Version 3.6) [Computer software]. Retrieved from http://www.povray.org/download/

[15] Drumm, P. V., and J. R.J Bennett. "A Comparison of RIST and ISOLDE Tantalum Targets and Geometries Used On-line at ISOLDE." Beam Interactions with Materials and Atoms 126 (1997): 121-24.

[16] Bennett, J. R.J. "Effusion in RNB Targets - a Simple Conductance Approach." Beam Interactions with Materials and Atoms 126 (1997): 146-49.

[17] Savchenko, I. V., and S. V. Stankus. "Thermal Conductivity and Thermal Diffusivity of Tantalum in the Temperature Range from 293 to 1800 K." Thermophysics and Aeromechanics 15.4 (2008): n. pag.

[18] Lettry, J. A. "Exotic Ion-Beams Targets and Sources." European Organization for Nuclear Research (CERN) (2000): n. pag. Web

[19] Koster, Ulli, and ISOLDE Collaboration. "On-line Separation of Short-lived Beryllium Isotopes." European Organization for Nuclear Research (CERN) (1998): n. pag. Web.

[20] Koster, Ulli. "ISOLDE Target and Ion Source Chemistry." Radiochim. Acta 89 (2001): 77-85. Web.

[21] Bergmann, U. C. "Light Exotic Isotopes: Recent Beam Developments and Physics Applications at ISOLDE." Nuclear Physics A 701 (2002): 363-68. Web

[22] Bricault, P. G. "Progress in Development of ISOL RIB Ion Sources and Targets for High Power." Cyclotrons and Their Applications 18 (2007): n. pag. Web.

[23] Bennett, J. R.J. "An Improved Analytical Model of Diffusion through the RIST Target." Beam Interactions with Materials and Atoms 204 (2003): 211-14. Web.

[24] M. Barbui. "Release Time Calculations for the SPES Direct UCx Target." The European Physical Journal of Special Topics 150 (2007): 275-76. Web.

[25] Andrighetto, A., and M. S. Leitner. "Multifoil UCx Target for the SPES Project - An Update." The European Physical Journal A 30 (2006): 591-601. Web.

[26] Densham, C. J. "Critical Parameters for the Delay Time of a RIB Target." Beam Interactions with Materials and Atoms 126 (1997): 154-59. Web.

[27] Bennett, J. R.J, and C. J. Densham. "The Design and Development of the RIST Target." Beam Interactions with Materials and Atoms 126 (1997): 117-20. Web.

[28] Beyer, G. J., and ISOLDE Collaboration. "The Role of Diffusion in ISOL Targets for the Production of Radioactive Ion Beams." European Organization for Nuclear Research (CERN) (2002): n. pag. Web.

[29] Egoriti, Luca. "Development and Benchmark of an Analytical Model for Isotope Release from ISOL Thin-foils Targets." Diss. Politechnico Di Milano, 2016. Print.

[30] Leitner, M. S. RIBO: A Monte Carlo Code to Optimize the Production of Radioactive Ion Beams. Proc. of Presentation at INFN-LNL, Legnaro, Italy. N.p.: n.p., 2006. Print.

[31] Mustapha, B., and J. A. Nolen. "Optimization of ISOL Targets Based on Monte Carlo Simulations of Ion Release Curves." Beam Interactions with Materials and Atoms 204 (2003): 286-92. Web.

[32] Bhowmick, Debasis. "Preparation and Optimization of Targets for the Production of Radioactive Ions at VECC." Nuclear Instruments and Methods in Physics Research 539 (2005): 54-62. Web.

[33] Zhang, Yan. "Simulation of Rare Isotope Release from ISOL Targets." Nuclear Instruments and Methods in Physics Research Section A: Accelerators, Spectrometers, Detectors and Associated Equipment (2010): n. pag. Web.

[34] Mustapha, B. "Simulations of Effusion from ISOL Target/ion Source Systems." Nuclear Instruments and Methods in Physics Research 521 (2004): 59-64. Web.

[35] Simulation Studies of Diffusion-Release and Effusive-Flow of Short-Lived Radioactive Isotopes. Proc. of 2005 Particle Accelerator Conference, Knoxville, Tennessee. N.p.: IEEE Xplore, 2005. Print.

[36] Densham, Christopher John. "Design and Development of a Tantalum Foil Target for the Production of High Intensity Radioactive Beams." Diss. U of Oxford, 2000. Print.

[37] Gottberg, A. "Target Materials for Exotic ISOL Beams." Nuclear Instruments and Methods in Physics Research Section B: Beam Interactions with Materials and Atoms 376 (2016): 8-15. Web.

Appendix A

.1 Version 1.0 of MATLAB Analysis Code

:

```
clear all, close all

% Load RIBO data
[event, x0, y0, z0, td, tPo, COLP, COL, teff, tT] = textread(...
    'C:\Users\Rohan\Documents\L3.5_times.out',...,
    '%f %f %f %f %f %f %f %f %f %f','headerlines', 1)
% Store in histogram
hist = histogram(tT,50,...
                    'Normalization','pdf')
% Compute sticking times
tT_stick = tT+COL*(10E-8)
hold on
hist = histogram(tT_stick,50,...
                    'Normalization','pdf')
% RIBO fit parameters
t = 0:0.0001:1;
t1 = 0.0017;
t2 = 0.06332;
f_eff = (1-exp(-t/t1)).*exp(-t/t2);

% integeral under curve
int = trapz(t,f_eff)
f_eff_norm = f_eff./int; % normalized
int_norm = trapz(t,f_eff_norm)

figure(1)
plot(t,f_eff_norm,'LineWidth',1.5);
legend('Effusion')
xlabel('Time [s]')
ylabel('Effusion release curve for Li^{7}')
xlim([0 .1])

% RELEASE FRACTION WITH HALF-LIFE %

li7 = Inf;
li11 = 8.75/1000;
li8 = 840.3/1000;
li9 = 178.3/1000;
A_relfrac = zeros(length(t),1);
B_relfrac = zeros(length(t),1);
```

```
C_relfrac = zeros(length(t),1);
D_relfrac = zeros(length(t),1);

%N_0 is from the production rate (FLUKA)
for i=2:length(t)
        int = trapz(t(1:i),f_eff_norm(1:i));
        int_halflife_li7 = int.*exp(-t(i)*log(2)/li7); %might have
    to make N_0 = max(counts)?
        A_relfrac(i,1) = int_halflife_li7;
        int_halflife_li8 = int.*exp(-t(i)*log(2)/li8); %might have
    to make N_0 = max(counts)?
        B_relfrac(i,1) = int_halflife_li8;
        int_halflife_li9 = int.*exp(-t(i)*log(2)/li9); %might have
    to make N_0 = max(counts)?
        C_relfrac(i,1) = int_halflife_li9;
        int_halflife_li11 = int.*exp(-t(i)*log(2)/li11); %might
    have to make N_0 = max(counts)?
        D_relfrac(i,1) = int_halflife_li11;
end

% here we calculate the release fraction for each isotope by the
% conventional method. For every timestep, we integrate the
    effusion curve
% and multiply by the associated decay loss factor. Then we divide
    by the
% integral under the effusion curve (without the decay loss factor)
    .

figure(3)
subplot(2,2,1)
plot(t,(A_relfrac),'g-','LineWidth',1.5)
title(['Release Fraction for Li^7: ' num2str(sum(A_relfrac)/sum(
    A_relfrac))],'FontSize', 15)
%xlabel('time (s)')
ylabel('Release Fraction')
grid on

subplot(2,2,2)
plot(t,(B_relfrac),'b-','LineWidth',2.5)
title(['Release Fraction for Li^8: ' num2str(sum(B_relfrac)/sum(
    A_relfrac))],'FontSize', 15)
%xlabel('time (s)')
%ylabel('Rf')
grid on

subplot(2,2,3)
plot(t,(C_relfrac),'y-','LineWidth',2.5)
title(['Release Fraction for Li^9: ' num2str(sum(C_relfrac)/sum(
    A_relfrac))],'FontSize', 15)
xlabel('Time (s)')
ylabel('Release Fraction')
grid on

subplot(2,2,4)
```

```
plot(t,(D_relfrac),'r-','LineWidth',2.5)
title(['Release Fraction for Li^{11}: ' num2str((sum(D_relfrac)/sum
    (A_relfrac)))],'FontSize', 15)
xlabel('Time (s)')
%ylabel('Rf')
xlim([0  0.1])
grid on

disp(sum(A_relfrac)*100/sum(A_relfrac))
disp(sum(B_relfrac)*100/sum(A_relfrac))
disp(sum(C_relfrac)*100/sum(A_relfrac))
disp(sum(D_relfrac)*100/sum(A_relfrac))

%%

% option to convert to custom bin size

%histogram properties
counts = h.Values;
binwidth = h.BinWidth;
edges = h.BinEdges;

%constant from real distribution obeying decaying exponential e.g.
    C*exp(t/t1)
binCentres = (edges(1:end-1) + edges(2:end))/2.0;
hold on
x_Cat= cat(2,0,counts)
y_Cat = cat(2,0,binCentres)

p1=plot(binCentres, counts,'^',...
                'MarkerEdgeColor','k',...
                'MarkerSize',5);
%Fit with statistical momenta from RIBO
hold on
t = 0:0.00001:0.25;
t1 = 0.00137;
t2 = 0.02511;
f = 38*(1-exp(-t/t1)).*exp(-t/t2);
p2=plot(t,f,'r','LineWidth',1.2);
grid on
xlabel('Time [seconds]','Interpreter','LaTex')
ylabel('Effusive Flux [counts/second]','Interpreter','LaTex')

l=legend([p1 p2],'Simulation Data','RIBO Fit')
set(l,'Interpreter','latex')

%%
% converting to cps to get small bin size
CPS = counts/binwidth

%plot(binCentres, CPS,'^',...
        %       'MarkerEdgeColor','k',...
         %      'MarkerSize',5);

```

```
% Custom bin size
%small bin size from 0 to 0.63*max(counts), larger bin size
    thereafter
%find corresponding t value for 0.63*max(counts)
hold on
Ft= max(CPS)*(1-exp(-t/t1)).*exp(-t/t2);
plot(t,Ft)
%find the t value that gives F=0.63*max(counts).
%this happens when the difference between Ft and 0.63*max(counts)
    is a minimum.
target = 0.63*max(CPS);
[difference, index_At_F_Equals_target] = min(abs(Ft-target));
ttarget = t(index_At_F_Equals_target);

%two different bin widths
num_small = 20;
num_big = 15;
times = tT
narrowBinCentres = linspace(0,ttarget,num_small);
wideBinCentres = linspace(ttarget, max(times),num_big);

%get edges half way in between.
narrowbinEdges = conv(narrowBinCentres, [0.5, 0.5], 'valid');
widebinEdges = conv(wideBinCentres, [0.5, 0.5], 'valid');

newbinEdges = horzcat(narrowbinEdges, widebinEdges);
figure()
%transparent histogram
h2 = histogram(times,newbinEdges,...
                    'FaceAlpha',0,...
                    'LineStyle', 'none',...
                    'Normalization','pdf');
hold on
%C from real distribution obeying decaying exponential e.g. C*exp(t
    /t1)
counts2 = h2.Values;
binwidth2 = h2.BinWidth;

edges2 = h2.BinEdges;
C2 = max(counts2);
h2binCentres = (newbinEdges(1:end-1) + newbinEdges(2:end))/2.0;
hold on
plot(h2binCentres, counts2,'^', 'MarkerEdgeColor','k',...
                'MarkerSize',5);
Ft= 5*(1-exp(-t/t1)).*exp(-t/t2);
plot(t,Ft,'LineWidth',1.2)
title('Custom bin size')

%% EMITTANCE PLOTS

file = fopen('C:\Users\Rohan\Documents\emitemit2.map');
tline = fgets(file);
var = [ ];
while ischar(tline) == 1
```

```
    lstr = fgetl(file);
    lnum = str2num(lstr);
    d = size(lnum,2);
    if d == 4
        var = [var; lnum];
    end
x1 = var(:,1)
u1u3 = var(:,2)
x2 = var(:,3)
u2u3 = var(:,4)
end

plot(x2,u2u3, '.', 'MarkerFaceColor','black', 'MarkerEdgeColor','
    black')
xlabel('dz (mm)','Interpreter','Latex')
ylabel('$\alpha_{z,y}$ (mrad)','Interpreter','Latex')
title('Vertical Emittance', 'Interpreter','Latex')

%% TRAJECTORY

[x0, y0, z0, t] = textread(...
   'C:\Users\Rohan\Documents\traj8.5.out',...,
   '%f %f %f %f', 'headerlines', 28);
plot3(x0,y0,z0,'blue','LineWidth',1)
xlabel('x','Interpreter','LaTex')
ylabel('y','Interpreter','LaTex')
zlabel('z','Interpreter','LaTex')
title('Trajectory of a $^{11}$Li nuclei effusing through 8.5 cm
    target (1.5$\times$10$^{6}$ timesteps)','Interpreter','LaTex')
grid on
hold on
```